Redox Biology 20 (2019) 182–194

Contents lists available at ScienceDirect

Redox Biology

journal homepage: www.elsevier.com/locate/redox

Research Paper

A novel platinum complex containing a piplartine derivative exhibits enhanced cytotoxicity, causes oxidative stress and triggers apoptotic cell death by ERK/p38 pathway in human acute promyelocytic leukemia HL-60 cells

Maiara de S. Oliveira[a], Marília I.F. Barbosa[b], Thiago Belarmino de Souza[c], Diogo R.M. Moreira[a], Felipe Terra Martins[d], Wilmer Villarreal[e], Rafael P. Machado[b], Antônio Carlos Doriguetto[b], Milena B.P. Soares[a,f], Daniel P. Bezerra[a,*]

[a] Gonçalo Moniz Institute, Oswaldo Cruz Foundation (IGM-FIOCRUZ/BA), Rua Waldemar Falcão, 121, Candeal, 40296-710 Salvador, Bahia, Brazil
[b] Institute of Chemistry, Federal University of Alfenas, Alfenas 37133-840, Minas Gerais, Brazil
[c] Department of Pharmacy, Federal University of Ouro Preto, Ouro Preto 35400-000, Minas Gerais, Brazil
[d] Institute of Chemistry, Federal University of Goiás, Goiânia 740011970, Goiás, Brazil
[e] Department of Chemistry, Federal University of São Carlos, São Carlos 13565-905, São Paulo, Brazil
[f] Center of Biotechnology and Cell Therapy, Hospital São Rafael, Salvador, Bahia 41253-190, Brazil

ARTICLE INFO

Keywords:
Piplartine
Piperlongumine
Platinum complex
Leukemia
Apoptosis
ROS
p38
ERK

ABSTRACT

Piplartine (piperlongumine) is a plant-derived compound found in some *Piper* species that became a novel potential antineoplastic agent. In the present study, we synthesized a novel platinum complex containing a piplartine derivative *cis*-[PtCl(PIP-OH)(PPh_3)$_2$]PF_6 (where, PIP-OH = piplartine demethylated derivative; and PPh_3 = triphenylphosphine) with enhanced cytotoxicity in different cancer cells, and investigated its apoptotic action in human promyelocytic leukemia HL-60 cells. The structure of PIP-OH ligand was characterized by X-ray crystallographic analysis and the resulting platinum complex was characterized by infrared, molar conductance measurements, elemental analysis and NMR experiments. We found that the complex is more potent than piplartine in a panel of cancer cell lines. Apoptotic cell morphology, increased internucleosomal DNA fragmentation, without cell membrane permeability, loss of the mitochondrial transmembrane potential, increased phosphatidylserine externalization and caspase-3 activation were observed in complex-treated HL-60 cells. Treatment with the complex also caused a marked increase in the production of reactive oxygen species (ROS), and the pretreatment with *N*-acetyl-L-cysteine, an antioxidant, reduced the complex-induced apoptosis, indicating activation of ROS-mediated apoptosis pathway. Important, pretreatment with a p38 MAPK inhibitor (PD 169316) and MEK inhibitor (U-0126), known to inhibit ERK1/2 activation, also prevented the complex-induced apoptosis. The complex did not induce DNA intercalation in cell-free DNA assays. In conclusion, the complex exhibits more potent cytotoxicity than piplartine in a panel of different cancer cells and triggers ROS/ERK/p38-mediated apoptosis in HL-60 cells.

1. Introduction

Leukemia is among the most usual cancer in the world, with around 352,000 new cases diagnosed in 2012, and was estimate about 265,500 deaths [1]. In special, the overall five-year survival rate for the acute myeloid leukemia was only 27% from 2006 to 2012 [2]. Although the arsenal of currently available chemotherapeutic agents represents a major advance in the treatment of leukemias, the development of new cytotoxic agents with less side-effect are need.

Piplartine (piperlongumine) is a plant-derived compound found in some *Piper* species that became a novel potential antineoplastic agent. Potent cytotoxicity, genotoxicity, antitumor, antiangiogenic and antimetastatic properties, in addition to presenting adequate bioavailability and safety profile have been attributed for this molecule and its derivatives [3–19]. Although its cytotoxic properties have been known for over three decades, the great interest in this molecule has arisen after

* Corresponding author.
E-mail address: daniel.bezerra@fiocruz.br (D.P. Bezerra).

https://doi.org/10.1016/j.redox.2018.10.006
Received 27 June 2018; Received in revised form 2 October 2018; Accepted 8 October 2018
Available online 12 October 2018

Table 1
Summary of crystal data and refinement statistics for the ligand PIP-OH.

structural formula[i]	$C_{16}H_{17}NO_5$
space group	$P2_1/c$
Z/Z'	4/1
a (Å)	7.3951(8)
b (Å)	15.1471(11)
c (Å)	13.3878(11)
β (°)	103.631(8)
V (Å)^3	1457.4(2)
calculated density (Mg/m^3)	1.382
θ range for data collection (°)	5.842–66.718
data collected	7451
unique reflections	2497
unique reflections with $I > 2\sigma I$)	1349
symmetry factor (R_{int})	0.1237
parameters refined	199
goodness-of-fit on F^2	1.077
final *R1* factor for $I > 2\sigma(I)$	0.0954
wR2 factor for all data	0.3261
largest Δρ peaks (e/Å^3)	0.368/− 0.207
CCDC deposit number	1,842,862

its cytotoxicity and ability to induce the production of reactive oxygen species (ROS) selectively in cancer cells were described [11,12]. Currently, the cytotoxic potential of piplartine and/or its derivatives have been extensively examined in different types of cancer, including leukemia [12,20–23].

The design of metallodrug-based compounds is an interesting strategy in medicinal chemistry [24–30]. The most important metallodrug-based compounds are the platinum-based antineoplastic agents. Moreover, platinum-based complexes are used in 50% of all chemotherapeutic regimens that include cisplatin, carboplatin and oxaliplatin [31]. Recently, two ruthenium-based piplartine complexes [Ru(piplartine)(dppf)(bipy)]$(PF_6)_2$ and [Ru(piplartine)(dppb)(bipy)]$(PF_6)_2$ (where, dppf = 1,1′-bis(diphenylphosphino) ferrocene; dppb = 1,4-bis(diphenylphosphino)butane and bipy = 2,2′-bipyridine) were obtained and displayed cytotoxicity more potent than piplartine in different cancer cell lines [32]; however, platinum-based complexes had not been previously designed with piplartine. In the present study, we

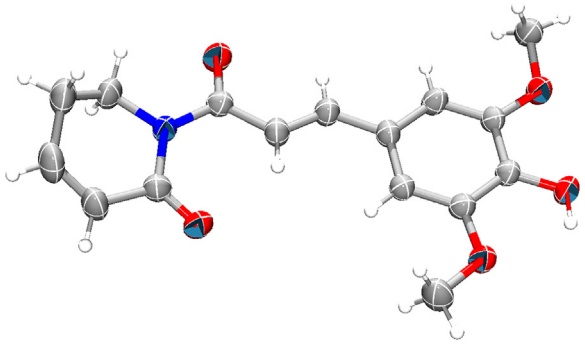

Fig. 2. Asymmetric unit of the ligand PIP-OH drawn with their 50% probability anisotropic ellipsoids (hydrogen atoms are arbitrary radius spheres).

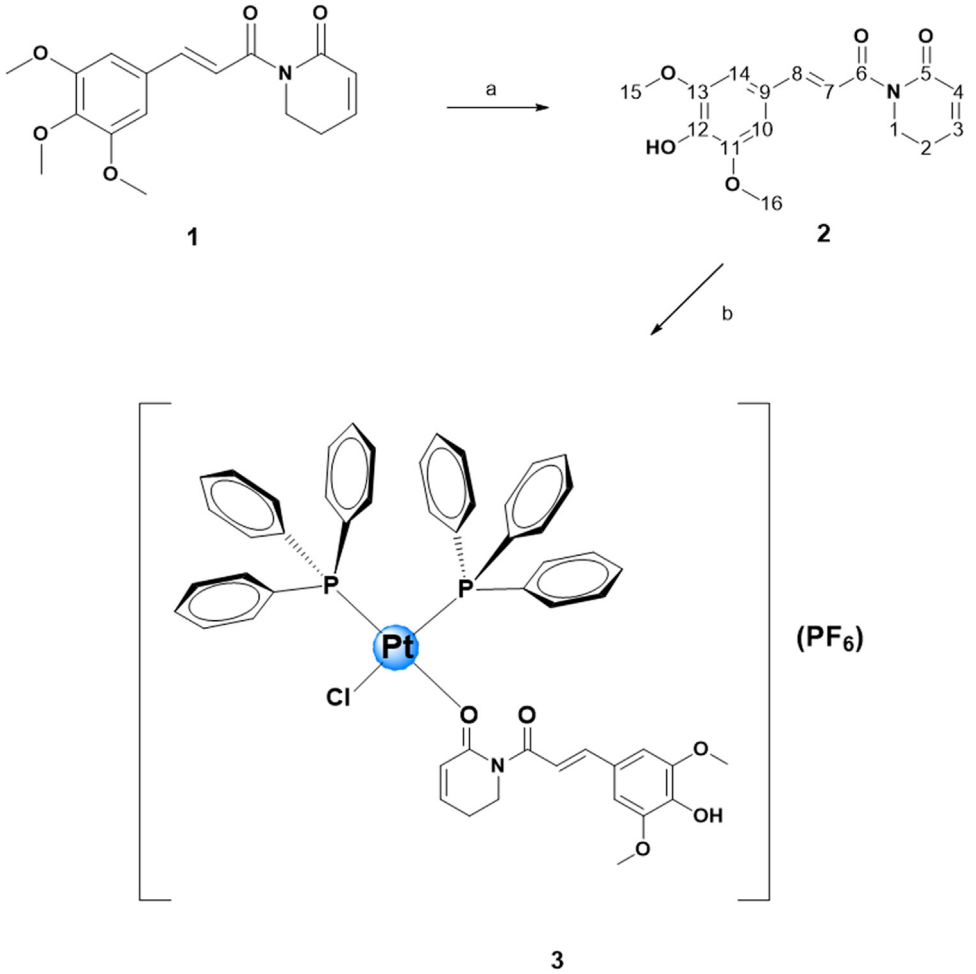

Fig. 1. Route for the synthesis of the complex *cis*-[PtCl(PIP-OH)$(PPh_3)_2$]PF_6. a) 1 – Al_3Cl_3, CH_2Cl_2, 0 °C; 2 – aqueous $NaHCO_3$, rt. b) $PtCl_2(PPH_3)_2$, NH_4PF_6, CH_2Cl_2, argon atmosphere.

Table 2
Chemical shifts (ppm) ^{1}H of PIP-OH and *cis*-[PtCl(PIP-OH)$(PPH_3)_2$]PF_6 (CPP) in CH_3OD.

	δ (ppm)		Δδ (ppm)
Hydrogen	**PIP-OH**	**CPP**	
1	2.49 (m)	2.54 (m)	0.05
2	3.97 (t)	4.00 (t)	0.03
3	5.98 (dt)	6.02 (dt)	0.04
4	7.05 (m)	7.09 (m)	0.04
7	7.60 (d)	7.64 (d)	0.04
8	7.31 (d)	7.34 (d)	0.03
10; 14	6.89(s)	6.93 (s)	0.04
15; 16	3.87 (s)	3.90 (s)	0.03

Table 3
Chemical shifts (ppm) $^{13}C\{^{1}H\}$ of PIP-OH and *cis*-[PtCl(PIP-OH)$(PPH_3)_2$]PF_6 (CPP) in CH_3OD.

	δ (ppm)		Δδ (ppm)
Carbon	**PIP-OH**	**CPP**	
1	42.96	43.09	0.13
2	25.69	25.79	0.10
3	148.16	148.32	0.16
4	125.92	126.01	0.09
5	167.72	167.86	0.14
6	170.76	170.90	0.14
7	120.34	120.46	0.12
9	127.29	127.40	0.11
8	145.25	145.34	0.09
10; 14	106.87	106.98	0.11
12	139.65	139.59	0.06
11; 13	149.41	149.52	0.11
15; 16	56.75	56.87	0.12

synthesized a novel platinum-based piplartine complex *cis*-[PtCl(PIP-OH)$(PPh_3)_2$]PF_6 (where, PIP-OH = piplartine demethylated derivative; and PPh_3 = triphenylphosphine) with enhanced cytotoxicity in different cancer cells, and its apoptotic action was investigated in human promyelocytic leukemia HL-60 cells.

2. Materials and methods

2.1. Synthesis

2.1.1. General

Elemental analyses were performed in a TruSpec CHNS-O model (Leco Instruments LTDA). The IR spectra were recorded on KBr pellets in the 4000–400/cm region in a Bomen–Michelson FT MB-102 instrument. The UV–vis spectra were recorded in CH_2Cl_2 solution, in a Hewlett Packard diode array – 8452A. All NMR experiments were recorded on a BRUKER, 300 MHz equipment, in a BBO 5 mm probe, at 298 K, and TMS for internal reference. For ^{1}H, $^{13}C\{^{1}H\}$, and $^{31}P\{^{1}H\}$ NMR spectra the CH_3OD and dimethyl sulfoxide (DMSO) were used as solvents. The splitting of proton, carbon and phosphorus resonances was reported as s = singlet, d = doublet, t = triplet, dt = double triplet and m = multiplet. Solvents were purified by standard methods. All chemicals used were of reagent grade or comparable purity. Piplartine (Cayman chemical, Ann Arbor, MI, USA) and $PtCl_2(PPh_3)_2$ (Sigma-Aldrich Co., Saint Louis, MO, USA) were used as received.

2.1.2. X-ray crystallography

Single crystal X-ray diffraction data were measured using a Bruker-AXS Kappa Duo diffractometer with an APEX II CCD detector (Cu Kα radiation, 296 K). Bruker programs SAINT and SADABS [33] were used for cell refinement and data indexing, integration and reduction. Multi-scan absorption correction was performed for our Cu Kα dataset [34].

Table 4
Cytotoxic activity of the complex *cis*-[PtCl(PIP-OH)$(PPh_3)_2$]PF_6 (CPP).

Cells	IC_{50} in μM				
	DOX	OXA	PIP	PIP-OH	CPP
Cancer cells					
HL-60	0.3	0.6	14.1	8.5	1.9
	0.3–0.4	0.1–0.8	8.3–19.8	4.9–15.0	1.2–3.1
K-562	0.3	1.0	18.6	23.2	1.1
	0.2–0.5	0.1–1.3	11.6–9,9	17.7–28.8	0.3–3.4
HCT116	0.1	4.1	5.4	11.4	4.8
	0.1–0.2	2.7–6.4	3.0–9.6	7.8–16.6	2.8–8.1
MCF-7	1.1	5.7	10.3	24.3	6.8
	0.3–3.5	3.3–9.4	4.5–14.3	16.4–29.6	3.8–12.4
HepG2	0.1	2.2	6.3	7.5	4.4
	0.1–0.2	1.3–3.8	4.5–8.8	6.6–8.5	3.1–6.2
HSC-3	0.3	3.1	14.1	16.3	1.0
	0.2–0.4	1.6–5.3	8.7–18.3	11.0–22.8	0,47–1,94
SCC-9	0.5	N.d.	16.5	23.5	6.2
	0.4–0.7		14.2–19.0	15.2–28.3	3.2–2.1
B16-F10	0.1	2.2	10.6	62.6	1.1
	0.1–0.2	1.2–4.1	6.9 – 16.1	45.9–85.4	0.5–2.5
Non-cancer cells					
MRC-5	1.5	1.3	17.3	14.0	7.5
	1.2–2.0	1.0–2.2	11.3–25.5	7.8–24.9	4.3–12.8
PBMC	5.1	9.4	34.2	54.2	10.3
	3.2–8.2	6.5–11.4	28.0–43.9	42.7–65.7	7.9–13.5

Data are presented as IC_{50} values in μM and their respective 95% confidence interval obtained by nonlinear regression from at the least three independent experiments performed in duplicate, measured by alamar blue assay after 72 h of incubation. Cancer cells: HL-60 (human promyelocytic leukemia); K-562 (human chronic myelogenous leukemia); HCT116 (human colon carcinoma); MCF-7 (human breast carcinoma); HepG2 (human hepatocellular carcinoma); HSC-3 (human oral squamous cell carcinoma); SCC-9 (human oral squamous cell carcinoma); and B16-F10 (mouse melanoma). Non-cancer cells: MRC-5 (human lung fibroblast) and PBMC (human peripheral blood mononuclear cells). Doxorubicin (DOX), oxaliplatin (OXA) and piplartine (PIP) were used as the positive controls. Piplartine demethylated derivative (PIP-OH) was also tested. N.d. Not determined.

Structure solution and refinement were performed using SHELXL-2014 [35] within the WinGX [36]. Artwork preparation were performed with ORTEP-3 [37]. Non-hydrogen and hydrogen atoms were refined anisotropically and isotropically, respectively. All hydrogens were added to their corresponding carbons and oxygen following a riding model with fixed bond angles and lengths (0.93 Å, 0.96 Å, 0.97 Å and 0.82 Å in aromatic, methyl, methylene and hydroxyl groups, respectively). Hydrogens had their isotropic atomic displacement parameters set to $1.2U_{iso}$(C), except in the case of methyl and hydroxyl groups where this value was $1.5U_{iso}$(C/O). The complete X-ray diffraction dataset for the ligand structure is available under CCDC number code shown in Table 1, wherein a summary of X-ray diffraction data is also presented.

2.1.3. (E)-(3′,-hydroxy-4′,5′-dimethoxycinnamoyl)-5,6-dihydro-2(1H)-pyridone

For (*E*)-(3′,-hydroxy-4′,5′-dimethoxycinnamoyl)-5,6-dihydro-2(1*H*)-pyridone (PIP-OH) synthesis, 0.3 g (0.945 mmol) of piplartine was dissolved in 10 mL of anhydrous dichloromethane and the solution was cooled to 0 °C. To this solution, 0.88 g (6.61 mmol) of anhydrous aluminum chloride was slowly added under magnetic stirring. After 5 min, the solution was warmed to room temperature and kept under stirring for 1 h, when 3 mL of saturated $NaHCO_3$ solution and 10 mL of water were added to the mixture. The resulting mixture was extracted with dichloromethane (3 × 20 mL) and the organic phase obtained was washed with saturated NaCl solution (3 × 20 mL), dried with anhydrous Na_2SO_4 and evaporated on a rotary evaporator. The obtained product was purified by column chromatography (eluent: hexane/ethyl acetate), providing 0.210 g of PIP-OH (73% yield). Anal. Calc. for $C_{16}H_{17}NO_3$: exp%. (calc%) C, 71.18 (70.83); H, 6.15 (6.32); N, 5.44

Table 5
Selectivity index of the complex *cis*-[PtCl(PIP-OH)(PPh_3)$_2$]PF_6 (CPP).

Cancer cells	Non-cancer cells									
	MRC-5					PBMC				
	DOX	OXA	PIP	PIP-OH	CPP	DOX	OXA	PIP	PIP-OH	CPP
HL-60	5	2.2	1.2	1.6	4	17	15.7	2.4	6.4	5.4
K-562	5	1.3	0.9	0.6	6.8	17	9.4	1.8	2.3	9.4
HCT116	15	0.3	3.2	1.2	1.6	51	2.3	6.3	4.8	2.2
MCF-7	1.4	0.2	1.7	0.6	1.1	4.6	1.7	3.3	2.2	1.5
HepG2	15	0.6	2.8	1.9	1.7	51	4.3	5.4	7.2	2.3
HSC-3	5	0.4	1.2	0.9	7.5	17	3.0	2.4	3.3	10.3
SCC-9	3	N.d.	1.1	0.6	1.2	10.2	N.d.	2.1	2.3	1.7
B16-F10	15	0.6	1.6	0.2	6.8	51	4.3	3.2	0.9	9.4

Data are presented the selectivity index (SI) calculated using the following formula: SI = IC_{50}[non-cancer cells]/IC_{50}[cancer cells]. Cancer cells: HL-60 (human promyelocytic leukemia); K-562 (human chronic myelogenous leukemia); HCT116 (human colon carcinoma); MCF-7 (human breast carcinoma); HepG2 (human hepatocellular carcinoma); HSC-3 (human oral squamous cell carcinoma); SCC-9 (human oral squamous cell carcinoma); and B16-F10 (mouse melanoma). Non-cancer cells: MRC-5 (human lung fibroblast) and PBMC (human peripheral blood mononuclear cells). Doxorubicin (DOX), oxaliplatin (OXA) and piplartine (PIP) were used as the positive controls. Piplartine demethylated derivative (PIP-OH) was also tested. N.d. Not determined.

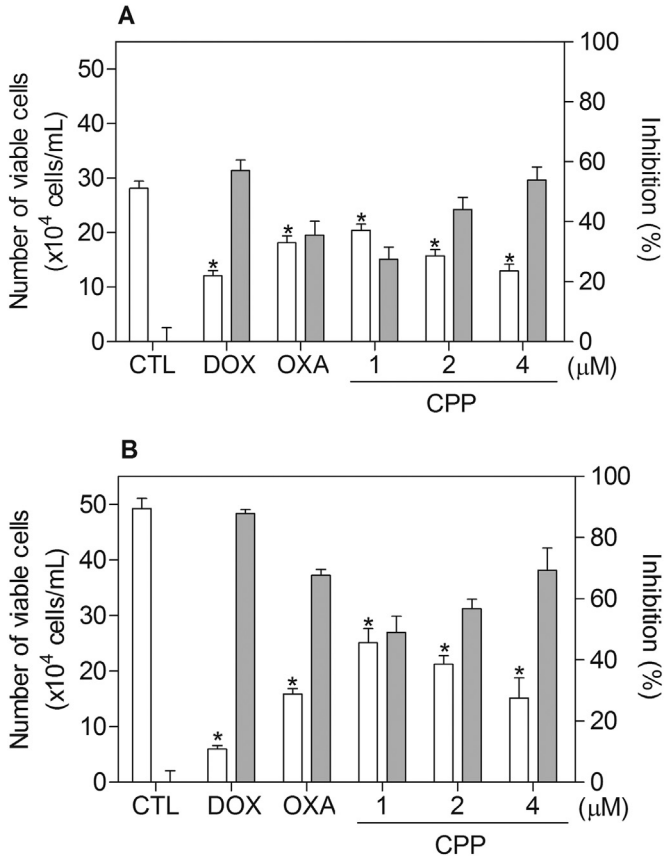

Fig. 3. Effect of the complex *cis*-[PtCl(PIP-OH)(PPh_3)$_2$]PF_6 (CPP) in the cell viability of HL-60 cells, as determined by the trypan blue staining after 24 (**A**) and 48 (**B**) h of incubation. The white bars represent number of viable cells (x10^{4}cells/mL) and the gray bars represent cell inhibition (%). The negative control (CTL) was treated with the vehicle (0.1% DMSO) used for diluting the compound tested. Doxorubicin (DOX, 2 μM) and oxaliplatin (OXA, 2.5 μM) were used as the positive controls. Data are presented as the means ± S.E.M. of three independent experiments performed in duplicate. * $P < 0.05$ compared with the negative control by ANOVA, followed by the Student Newman-Keuls Test.

(5.16). ^{1}H NMR (300 MHz; CH_3OD, 298 K): 7.60 (d, 12.0 Hz, 1H, H-7), 7.31 (d, 12.0 Hz, 1H, H-8), 7.05 (m, 1 H, H-7), 6.89 (s, 2H, H-10, H-14), 5.98 (dt, 9.9 and 1.9 Hz, 1H, H-3), 3.97 (t, 6.5, 2H, H-2), 3.87 (s, 6H, OMe-15 and 16), 2.49 (m, 2H, H-1). ^{1}H NMR (300 MHz; DMSO-*d*6, 298 K): 9.00 (s, 1H, OH). ^{13}C{^{1}H} NMR (300 MHz; CH_3OD): 42.96 (C-1), 25.69 (C-2), 148.16 (C-3), 125.92 (C-4), 167.62 (C-5), 170.76 (C-6), 120.34 (C-7), 127.29 (C-9), 145.25 (C-8), 106.87 (C-10, C-14), 139.65 (C-12), 149.41 (C-11, C-13) and 56.75 (C-15, C-16). UV–Vis (CH_2Cl_2, 4.65 × 10^{-5} M): λ/nm (ε/M/L/cm) 344 (24,012).

2.1.4. *Cis-[PtCl(PIP-OH)(PPh_3)$_2$]PF_6*

The complex *cis*-[PtCl(PIP-OH)(PPh_3)$_2$]PF_6 was prepared by reacting 0.05 g (0.06 mmol) of $PtCl_2(PPh_3)_2$ with 0.017 g (0.06 mmol) of PIP-OH ligand and 0.02 g (0.13 mmol) of NH_4PF_6 in 20 mL of dichloromethane previously degassed. The solution was kept under inert argon atmosphere and it was stirred for 24 h. The final solution was concentrated to ca. 2 mL, and 10 mL of hexane was added to precipitate a yellow powder. The solid was filtered off, washed with hexane and then dried under vacuum, providing 0.049 g of *cis*-[PtCl(PIP-OH)(PPh_3)$_2$]PF_6 (66% yield). Anal. Calc. for $C_{52}H_{47}ClF_6NO_3P_3Pt$: exp%. (calc%) C, 52.82 (53.32); H, 4.33% (4.04%); N, 1.44% (1.20%). Molar conductance (S/cm^2/mol, acetone) 60.31. IR (/cm) 1667 (νC=O). ^{31}P{^{1}H} NMR (121.50 MHz, CH_3OD, 298 K): δ (ppm) 13.8 and 6.19 (d) ($^2J_{P\text{-}P}$ = 19.4 Hz). ^{1}H NMR (300 MHz, CH_3OD, 298 K): *δ* (ppm): 7.64 (d, 15.0 Hz, 1 H, H-7), 7.34 (d, 15.0 Hz, 1H, H-8), 7.09 (m, 1H, H4), 6.93 (s, 2H, H-10, H-14), 6.02 (dt, 9.9 and 2.1 Hz, 1H, H-3), 4.00 (t, 6.5, 2H, H-2), 3.90 (s, 6H, OMe-15 and 16), 2.54 (m, 2H, H-1). ^{13}C{^{1}H} NMR (300 MHz, CH_3OD, 298 K): 43.09 (C-1), 25.79 (C-2), 148.32 (C-3), 126.07 (C-4), 167.86 (C-5), 170.90 (C-6), 120.46 (C-7), 145.34 (C-8), 127.40 (C-9), 106.98 (C-10, C-14), 149.52 (C-11, C-13), 139.59 (C12) and 56.87 (C-15, C16). UV–Vis (CH_2Cl_2, 5.18 × 10^{-5} M): λ/nm (ε/M/L/cm) 325 (21,035).

2.2.1. *Cell culture*

A total of eight cancer cell lines and two non-cancer cells were used in this study and the detailed are shown in Table S1. Primary cell culture of peripheral blood mononuclear cells (PBMC) were obtained with informed consent (# 031019/2013). Cells were cultured in RPMI-1640 medium (Gibco-BRL, Gaithersburg, MD, USA) with 10% fetal bovine serum (Life, Carlsbad, CA, USA), 2 mM L-glutamine (Vetec Química Fina, Duque de Caxias, RJ, Brazil) and 50 μg/mL gentamycin (Life, Carlsbad, CA, USA). Adherent cells were collected by treatment with 0.25% trypsin EDTA solution (Gibco-BRL, Gaithersburg, MD, USA). All cell lines were cultured in flasks at 37 °C in 5% CO_2 and subcultured every 3–4 days to maintain exponential growth. All cell lines were tested for mycoplasma using a mycoplasma stain kit (Sigma-Aldrich Co.) to validate the use of cells free from contamination. Cell viability was assessed by trypan blue exclusion assay for all experiments and over 90% of the cells were viable at the beginning of the culture.

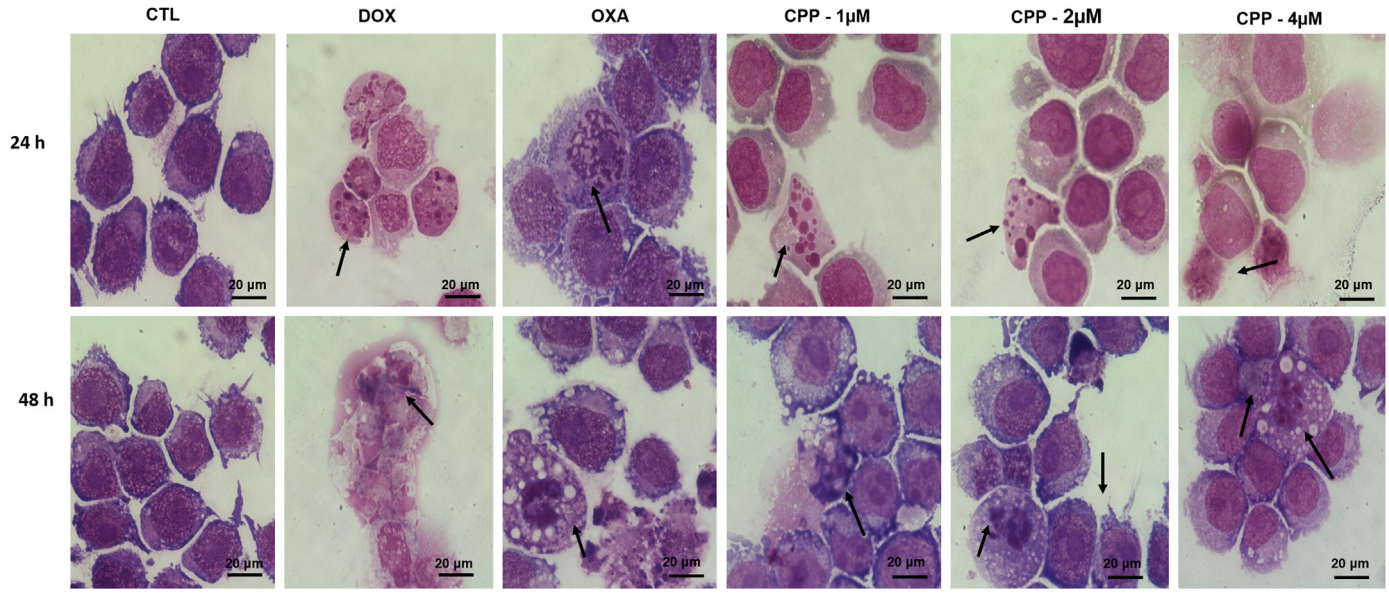

Fig. 4. Effect of the complex *cis*-[PtCl(PIP-OH)(PPh_3)$_2$]PF_6 (CPP) in the morphology of HL-60 cells after 24 and 48 h of incubation. The cells were stained with may-grunwald-giemsa and examined by light microscopy (bar = 20 μm). Arrows indicate cell shrinkage or cells with fragmented DNA. The negative control (CTL) was treated with the vehicle (0.1% DMSO) used for diluting the compound tested. Doxorubicin (DOX, 2 μM) and oxaliplatin (OXA, 2.5 μM) were used as the positive controls.

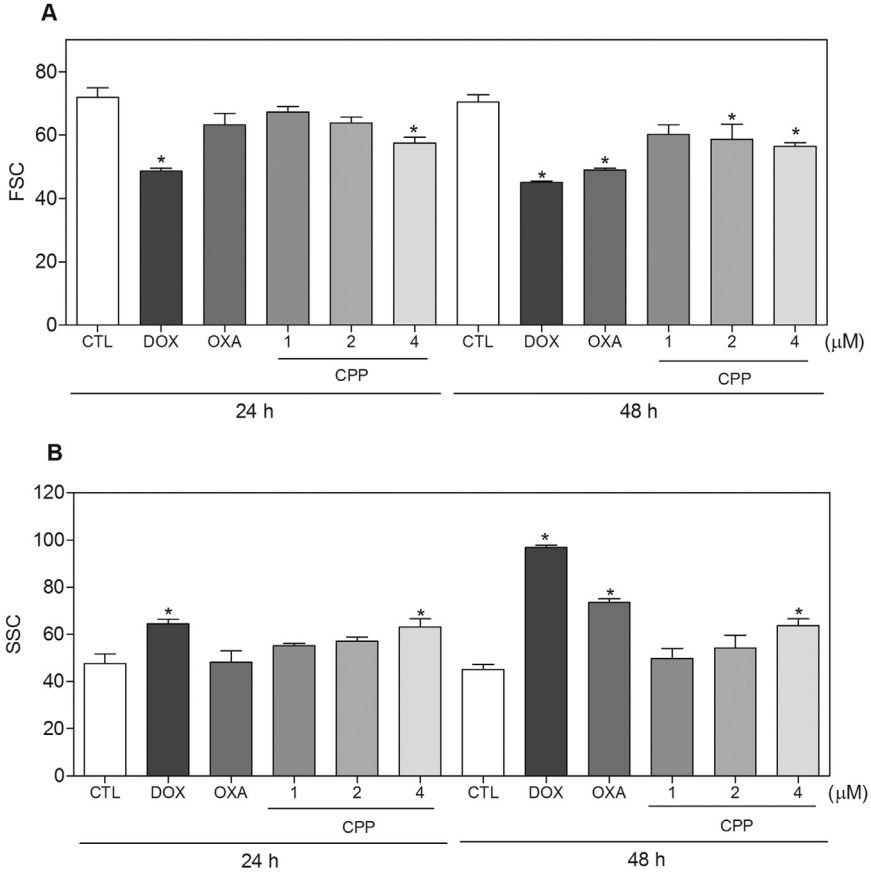

Fig. 5. Effect of the complex *cis*-[PtCl(PIP-OH)(PPh_3)$_2$]PF_6 (CPP) in the morphology of HL-60 cells after 24 and 48 h of incubation. (**A**) Quantification of forward light scatter (FSC) determined by flow cytometry. (**B**) Quantification of side scatter (SCC) determined by flow cytometry. The negative control (CTL) was treated with the vehicle (0.1% DMSO) used for diluting the compound tested. Doxorubicin (DOX, 2 μM) and oxaliplatin (OXA, 2.5 μM) were used as the positive controls. Data are presented as the means ± S.E.M. of three independent experiments performed in duplicate. Ten thousand events were evaluated per experiment and cellular debris was omitted from the analysis. $^*P < 0.05$ compared with the negative control by ANOVA, followed by the Student-Newman-Keuls test.

2.2.2. Alamar blue assay

The alamar blue assay was used to quantify the cell viability and was performed following the procedure that was previously described [38–40]. Negative controls received the vehicle that was used for diluting the compound tested. Doxorubicin (purity ≥ 95%, doxorubicin hydrochloride, Laboratory IMA S.A.I.C., Buenos Aires, Argentina), oxaliplatin (Sigma-Aldrich Co.) and piplartine (purity > 98%, Cayman Chemical) were used as the positive controls. The drug effect was quantified as the percentage of control absorbance and the half-maximal (50%) inhibitory concentration (IC_{50}) was calculated to each compound. The selectivity index was calculated using the following formula: selectivity index = IC_{50} [non-cancer cells]/IC_{50} [cancer cells].

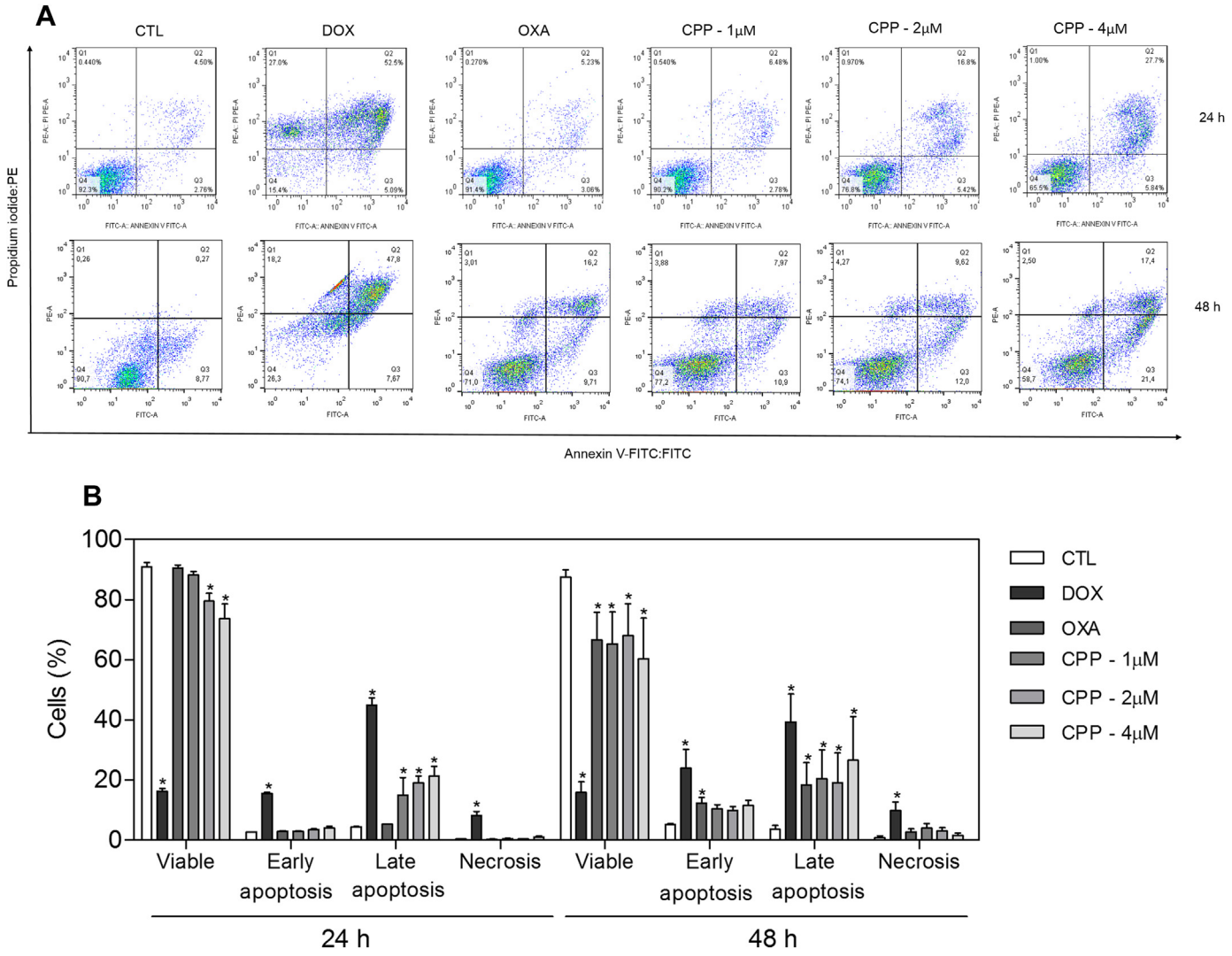

Fig. 6. Effect of the complex *cis*-[PtCl(PIP-OH)(PPh_3)$_2$]PF_6 (CPP) in the induction of apoptosis in HL-60 cells after 24 and 48 h of incubation as determined by flow cytometry using annexin V-FITC/PI staining. (**A**) Representative flow cytometry dot plots show the percent cells in the viable, early apoptotic, late apoptotic and necrotic stage. (**B**) Quantification of apoptotic HL-60 cells. The negative control (CTL) was treated with the vehicle (0.1% DMSO) used for diluting the compound tested. Doxorubicin (DOX, 2 μM) and oxaliplatin (OXA, 2.5 μM) were used as the positive controls. Data are presented as the means ± S.E.M. of three independent experiments performed in duplicate. Ten thousand events were evaluated per experiment and cellular debris was omitted from the analysis. * $P < 0.05$ compared with the negative control by ANOVA, followed by the Student-Newman-Keuls test.

2.2.3. Morphological analysis

Cell morphology was analyzed using May-Grunwald-Giemsa staining. Morphological alterations were observed by light microscopy using Image-Pro software. Moreover, light scattering features was measured by flow cytometry, and the forward light scatter (FSC) and the side scatter (SCC) were quantified. For flow cytometry analyses, 10^4 events were recorded per sample using a BD LSRFortessa cytometer along with BD FACSDiva Software (BD Biosciences) and Flowjo Software 10 (Flowjo LCC). The cellular debris was omitted from the analysis.

2.2.4. Annexin-V/PI staining assay

For apoptosis quantification, we used the FITC Annexin V Apoptosis Detection Kit I (BD Biosciences, San Jose, CA, EUA) and the analysis were performed according to the manufacturer's instructions and cell fluorescence was measured by flow cytometry as described above. For protection assays, Jun kinase (JNK/SAPK) inhibitor (SP 600125; Cayman Chemical), p38 MAPK inhibitor (PD 169316; Cayman Chemical), mitogen-activated protein kinase kinase (MEK) inhibitor (U-0126; Cayman Chemical) and the antioxidant *N*-acetyl-L-cysteine (NAC, Sigma-Aldrich Co.) were used. Briefly, the cells were pretreated for 2 h with 5 μM SP 600125, 5 μM PD 169316, 5 μM U-0126 or 5 mM NAC, followed by incubation with 4 μM of the complex for 48 h. Then, the cells were trypsinized, and apoptosis quantification assay was performed as described above.

2.2.5. Analysis of the mitochondrial transmembrane potential

Mitochondrial transmembrane potential was investigated using the retention of the dye rhodamine 123 and was evaluated following the procedure that was previously described [41]. Cells were incubated with rhodamine 123 (5 μg/mL, Sigma-Aldrich Co.) at 37 °C for 15 min in the dark and washed with saline. The cells were then incubated again in saline at 37 °C for 30 min in the dark and cell fluorescence was analyzed by flow cytometry as described above.

2.2.6. Caspase-3 activation assay

A caspase-3 colorimetric assay kit (Sigma-Aldrich Co.) was used to investigate caspase-3 activation and the analysis was performed according to the manufacturer's instructions. Total protein quantification was performed by Bradford method. Absorbance at 405 nm was

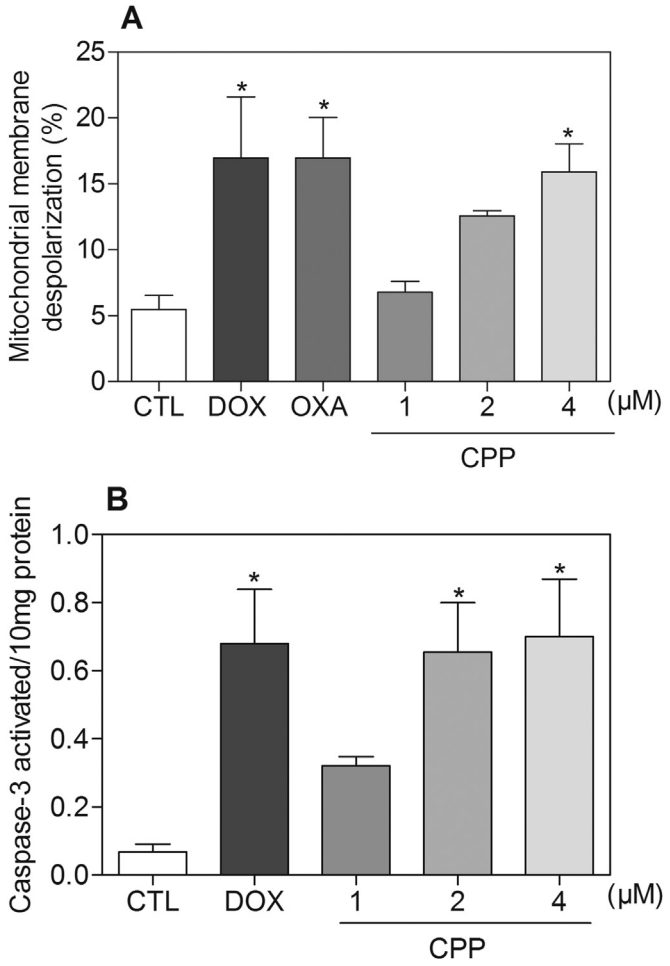

Fig. 7. Effect of the complex *cis*-[PtCl(PIP-OH)(PPh_3)$_2$]PF_6 (CPP) in the mitochondrial membrane potential and caspase-3 activity in HL-60 cells. (**A**) Mitochondrial membrane potential was determined by flow cytometry using rhodamine 123 staining after 24 h of incubation. (**B**) Caspase-3 activity was determined by colorimetric assay after 48 h of incubation. The negative control (CTL) was treated with the vehicle (0.1% DMSO) used for diluting the compound tested. Doxorubicin (DOX, 2 μM) and oxaliplatin (OXA, 2.5 μM) were used as the positive controls. Data are presented as the means ± S.E.M. of three independent experiments performed in duplicate. For flow cytometry analysis, 10,000 events were evaluated per experiment and cellular debris was omitted from the analysis. $^*P < 0.05$ compared with the negative control by ANOVA, followed by the Student-Newman-Keuls test.

measured using the SpectraMax 190 Microplate Reader (Molecular Devices, Sunnyvale, CA, EUA). The results were expressed as specific activity of caspase-3 per 10 mg protein.

2.2.7. Internucleosomal DNA fragmentation and cell cycle distribution

The internucleosomal DNA fragmentation and cell cycle distribution were determined using propidium iodide (PI) (Sigma-Aldrich Co.) in permeabilized cells and was performed following the procedure that was previously described [42]. Cell fluorescence was measured by flow cytometry as described above.

2.2.8. Analysis of intracellular reactive oxygen species levels

The levels of ROS were measured using 2′,7′-dichlorofluorescin diacetate (DCFH-DA, Sigma-Aldrich Co.) and was evaluated following the procedure that was previously described [43]. Cell fluorescence was measured by flow cytometry as described above.

2.2.9. DNA intercalation assay

DNA intercalation was assessed by examining the ability of the complex to displace ethidium bromide from calf thymus DNA (ctDNA, Sigma-Aldrich Co.) [44]. The DNA intercalation assay was conducted in 96-well plate (100 μL) and contained 15 μg/mL ctDNA, 1.5 μM ethidium bromide and 5, 10 and 20 μM of the complex in saline solution. The vehicle (0.1% DMSO) used for diluting the compounds tested was used as the negative control. Doxorubicin (10 μM) was used as the positive control. Fluorescence was measured using excitation and emission wavelengths of 320 and 600 nm, respectively using the spectraMax Microplate Reader (Molecular Devices, Sunnyvale, CA, EUA).

2.2.10. Statistical analysis

Data are presented as mean ± S.E.M. or IC_{50} values with their 95% confidence intervals obtained by nonlinear regression. Differences between experimental groups were compared using analysis of variance (ANOVA) followed by the Student–Newman–Keuls test ($p < 0.05$). All statistical analyses were performed using GraphPad Prism (Intuitive Software for Science, San Diego, CA, USA).

3. Results

3.1. Synthesis of the complex cis-[PtCl(PIP-OH)(PPh_3)$_2$]PF_6

Initially, the synthesis of piplartine demethylated derivative PIP-OH was obtained as depicted in Fig. 1 by using a method described by Adams et al. [11]. The ligand was characterized by ^{1}H and ^{13}C{^{1}H} NMR, UV–Vis and IR spectroscopy (Figs. S1–S3), in addition to elemental analysis, which was in agreement to the proposed composition. Important, the ligand PIP-OH had its structure determined by X-ray crystallography (Fig. 2), showing the presence of hydroxyl group.

The reaction of PIP-OH ligand with the platinum precursor $PtCl_2(PPh_3)_2$ resulted in a product of formula *cis*-[PtCl(PIP-OH)(PPh_3)$_2$]PF_6, by one chloride exchange. The ligand PIP-OH acted as monodentade specie, coordinating with the platinum atom through its carbonyl group (position C-5) (Fig. 1). Despite the presence of the OH group (C-12), the coordination to the metallic center occurred by the carbonyl (C-5). This is probably due to the involvement of the lone pair of electrons in the electronic resonance of phenyl ring, in which it is attached, reducing its basicity. With respect to C=O (C-5), a carbonyl of a lactam, the lone pair of electrons on the N atom delocalized with the carbonyl group, increases its basicity, and makes O (C-5) atom a softer base site, thus, the interaction with Pt^{2+}, a soft acid, is more effective. Resonance effects also act on the carbonyl (C-6), however it suffers from steric hindrance that makes O-Pt interaction unfeasible. Moreover, steric effects also contribute to non-coordination by hydroxyl (C-12). Similar behavior was observed for piplartine when it was coordinated to VO(II) and Ru(II) ions [32]. The elemental analyses agree well with the proposed formulation for the obtained complex. The molar conductance value, measured in acetone, at room temperature, was 60.3 μS/cm, revealing 1:1-type compounds [45].

The ^{31}P{^{1}H} NMR spectra of the complex in CH_3OD presented a typical AX spin system, indicating the magnetic nonequivalence of the two phosphorus atoms in *cis* position, in which one is *trans* to the Cl^- ligand and the other is *trans* to the O of the carbonyl (C-5) ligand (Fig. 4S). The chemical shifts and coupling constants ($^2J_{P\text{-}P}$) are shown in the experimental section, and are in agreement with P-Pt-O. The ^{31}P{^{1}H} NMR chemical shifts was different from starting material $PtCl_2(PPh_3)_2$, suggesting that the presence of PIP-OH ligand coordinated to the metal shifted the electron density of the phosphorus atoms of the PPh_3 ligand. Also, were observed coupling P-^{195}Pt by the satellites presence (Fig. 4S).

The ^{1}H NMR spectra of the complex, in CH_3OD, display signals correspondent to the hydrogen atoms of triphenylphosphine and PIP-OH ligands (Fig. 5S). As expected, it was observed a consistent shift of signals for downfield region for the complex when compared to metal-

Table 6
Effect of the complex *cis*-[PtCl(PIP-OH)(PPh_3)$_2$]PF_6 (CPP) in the cell cycle distribution of HL-60 cells.

Treatment	Concentration (μM)	DNA content (%)			
		Sub-G_0/G_1	G_0/G_1	S	G_2/M
24 h of incubation					
CTL	–	12.1 ± 1.2	49.7 ± 3.6	15.1 ± 1.6	16.5 ± 0.5
DOX	2	57.2 ± 2.5*	19.9 ± 2.5*	6.6 ± 1.6*	8.9 ± 1.5
OXA	2.5	20.7 ± 2.9*	29.1 ± 2.4*	12.6 ± 2.5	28.1 ± 2.6*
CPP	1	25.0 ± 1.6*	32.0 ± 5.4*	10.5 ± 1.8	13.2 ± 2.9
	2	29.2 ± 0.9*	34.3 ± 2.9*	10.3 ± 1.1	15.0 ± 2.5
	4	26.2 ± 4.1*	26.7 ± 4.6*	10.1 ± 1.4	15.3 ± 2.6
48 h of incubation					
CTL	–	6.3 ± 0.7	58.5 ± 3.1	14.1 ± 1.3	17.0 ± 1.6
DOX	2	65.5 ± 2.8*	21.9 ± 3.0*	6.5 ± 0.6*	3.8 ± 0.9*
OXA	2.5	24.8 ± 1.9*	42.9 ± 2.8	13.2 ± 0.8	23.4 ± 2.6*
CPP	1	19.8 ± 1.4*	49.7 ± 2.2	12.3 ± 1.6	14.5 ± 0.9
	2	25.8 ± 3.8*	48.5 ± 3.1	14.3 ± 0.8	14.1 ± 1.5
	4	27.3 ± 7.0*	41.9 ± 8.6	8.0 ± 2.0*	12.8 ± 2.8

Data are presented as the mean ± S.E.M. of three independent experiments performed in duplicate. The negative control (CTL) was treated with the vehicle (0.1% DMSO) used for diluting the compound tested. Doxorubicin (DOX) and oxaliplatin (OXA) were used as the positive controls. Ten thousand events were evaluated per experiment and cellular debris was omitted from the analysis.

* $P < 0.05$ compared with the negative control by ANOVA followed by Student Newman-Keuls Test.

free ligand (Table 2). The small disbanding effect occurs because Pt^{2+}, has a d8 configuration, which does not exert an electron withdrawing effect as significant as occurs with more electron deficient metals. Other aromatic hydrogen atom resonances were in the range 7.1–7.7 ppm which were attributed to the protons present in the aromatic phosphine (Fig. 5S). The $^{13}C\{^1H\}$ NMR spectra of the complex display signals around 167.96– 170.90 ppm, typical of the C=O group. This signal is deshielding in comparison to the metal-free piplartine ligand, where they occur at 167.72 and 170.76 ppm, indicating that oxygen of carboxyl group is coordinated to the metal (Table 3 and Fig. S6).

The infrared spectra of the complex show the typical ν(C=O) carbonyl stretching frequency at 1667/cm while the metal-free piplartine ligand displays this stretching mode at 1659/cm. The difference between the metal-free and coordinated ν(C=O) piplartine values ($\Delta\nu$ = 8/cm) is indicative of coordination, through the carbonyl group [46]. Strong bands are present in the spectra of the piplartine and of the precursor complexes in the region of 1600–1300/cm, characteristics of νC=C stretching vibrations. Also, νPt-P and νPt-O stretching bands in the range of 550–500/cm were observed. The characteristic P–F stretch of the PF_6^- counter-ion is at 843/cm (Fig. 7S). The UV–vis spectra of the complex displayed a large band associated with the presence of coordinated PIP-OH, at 320 nm, while free piplartine presented a band at 345 nm, corresponding to π–π^* transitions from the PIP-OH and phosphine ligands (Fig. 8S).

Finally, time-dependent $^{31}P\{^1H\}$ NMR experiments in solution were carried out to evaluate the stability of the complexes. The complexes were diluted in DMSO and analyzed from 0 to 48 h (Fig. 9S). The $^{31}P\{^1H\}$ NMR spectra revealed that after 1 h of incubation, there was a significant dissociation of PIP-OH ligand from the metal complex, while after 48 h, most the PIP-OH was dissociated from the metal complex.

3.2. The complex cis-[PtCl(PIP-OH)(PPh_3)$_2$]PF_6 exhibits more potent cytotoxicity than piplartine in a panel of cancer cells

The cytotoxicity of the complex *cis*-[PtCl(PIP-OH)(PPh_3)$_2$]PF_6 in eight cancer cell lines (HL-60, K-562, HCT116, MCF-7, HepG2, HSC-3, SCC-9 and B16-F10) and two non-cancer cells (MRC-5 and PBMC) was evaluated using the alamar blue assay after 72 h of incubation. Table 4 shows the IC_{50} obtained. The complex presented enhanced cytotoxicity to different cancer cells, with IC_{50} values ranging from 1.0 to 6.8 μM for cancer cell lines HSC-3 and MCF-7, respectively. Piplartine presented IC_{50} values ranging from 5.4 to 18.6 μM for cancer cell lines HCT116 and K-562, respectively, while the piplartine demethylated derivative PIP-OH presented IC_{50} values ranging from 7.5 to 62.6 μM for cancer cell lines HepG2 and B16-F10, respectively. The platinum precursor *cis*-[$PtCl_2(PPh_3)_2$] was not cytotoxic at the concentrations tested ($IC_{50} > 31.6$ μM). The complex was more potent than piplartine in HL-60 (7.4-fold), K-562 (16.9-fold), HCT116 (1.1-fold), MCF-7 (1.5-fold), HepG2 (1.4-fold), HSC-3 (14.1-fold), SCC-9 (2.7-fold) and B16-F10 (9.6-fold), and more potent than PIP-OH in HL-60 (4.5-fold), K-562 (21.1-fold), HCT116 (2.4-fold), MCF-7 (3.6-fold), HSC-3 (1.7-fold), SCC-9 (3.8-fold) and B16-F10 (56.9-fold). Doxorubicin, used as positive control, presented IC_{50} values ranging from 0.1 to 1.1 μM for cancer cell lines HCT116 and MCF-7, respectively. Oxaliplatin, also used as positive control, presented IC_{50} values ranging from 0.6 to 5.7 μM for cancer cell lines HL-60 and MCF-7, respectively.

The IC_{50} value for non-cancer cells was 7.5 and 10.3 μM for the complex, 17.3 and 34.2 μM for piplartine, and 14.0 and 54.2 μM for PIP-OH in MRC-5 and PBMC cells, respectively. The platinum precursor *cis*-[$PtCl_2(PPh_3)_2$] was not cytotoxic to non-cancer cells at the concentrations tested ($IC_{50} > 31.6$ μM). In addition, the IC_{50} value in non-cancer cells was 1.5 and 5.1 μM for doxorubicin, and 1.3 and 9.4 μM for oxaliplatin in MRC-5 and PBMC cells, respectively. Table 5 shows the selectivity index calculated. The complex exhibited selectivity index similar to piplartine, PIP-OH, doxorubicin and oxaliplatin to most of the cell lines tested.

In a new set of experiment, human promyelocytic leukemia HL-60 cell line was used as a cellular model, since it was among the most sensitive cell lines to the complex tested. Moreover, this cell line is often used as cellular model in the study of the mechanism of action of new compounds [5,28,47,48]. Therefore, the cytotoxicity of the complex was confirmed by TBE assay in HL-60 cells after 24 and 48 h of incubation. The complex significantly reduced ($p < 0.05$) the number of viable cells (Fig. 3). At concentrations of 1, 2 and 4 μM, the complex reduced the number of viable cells by 27.4%, 44.1% and 53.9% after 24 h, and 49.0%, 56.8% and 69.3% after 48 h, respectively. Doxorubicin at 2 μM reduced the number of viable cells by 57.1 after 24 h, and 87.9 after 48 h, and oxaliplatin at 2.5 μM reduced the number of viable cells by 35.6 after 24 h, and 67.7 after 48 h. No significant ($p > 0.05$) increase in the number of non-viable cells was observed.

3.3. The complex cis-[PtCl(PIP-OH)(PPh_3)$_2$]PF_6 causes ROS/ERK/p38-mediated apoptosis in HL-60 cells

Cell morphology of complex-treated HL-60 cells presented reduction in the cell volume, chromatin condensation and fragmentation of the

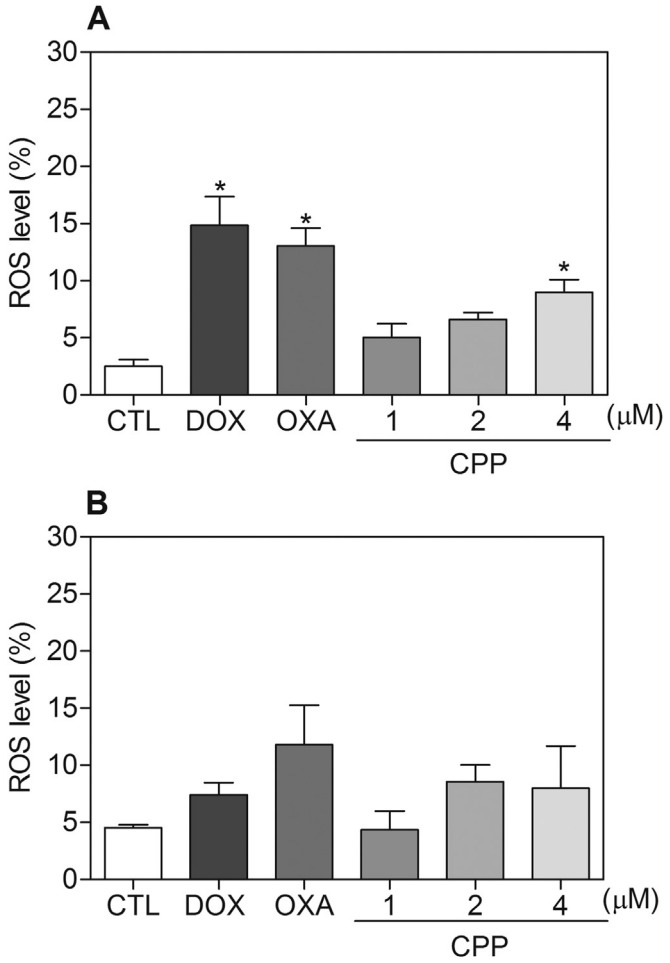

Fig. 8. Effect of the complex *cis*-[PtCl(PIP-OH)(PPh_3)$_2$]PF_6 (CPP) in the levels of reactive oxygen species (ROS) of HL-60 cells determined by flow cytometry using DCFH-DA staining after 1 (**A**) and 3 (**B**) h of incubation. The negative control (CTL) was treated with the vehicle (0.1% DMSO) used for diluting the compound tested. Doxorubicin (DOX, 2 μM) and oxaliplatin (OXA, 2.5 μM) were used as the positive controls. Data are presented as the means ± S.E.M. of three independent experiments performed in duplicate or triplicate. Ten thousand events were evaluated per experiment and cellular debris was omitted from the analysis. * $P < 0.05$ compared with the negative control by ANOVA, followed by the Student Newman-Keuls Test.

nuclei after 24 and 48 h of incubation (Fig. 4). Doxorubicin and oxaliplatin also induced cell shrinkage, chromatin condensation and nuclear fragmentation. Moreover, the complex, doxorubicin and oxaliplatin caused cell shrinkage, as observed by the decrease in FSC, and nuclear condensation, as indicated by a transient increase in SCC, both assessed by flow cytometry (Fig. 5). In addition, analysis of annexin V-FITC and PI double staining was performed by flow cytometry to measure the percentage of cells in viable, early apoptotic, late apoptotic and necrotic stages after 24 and 48 h of incubation (Fig. 6). The treatment with the complex resulted in increasing in apoptotic cells with more pronounced effect after 48 h of incubation ($p < 0.05$). Similarly, doxorubicin and oxaliplatin also caused increase in apoptotic cells ($p < 0.05$). Moreover, the treatment with the complex induced loss of the mitochondrial transmembrane potential after 24 h of incubation ($p < 0.05$) (Fig. 7**A**), as assessed by the incorporation of rhodamine 123 using flow cytometry, and significantly increased the caspase-3 activation after 48 h of incubation ($p < 0.05$) (Fig. 7**B**), as measured by colorimetric assay using DEVD-pNA as the substrate. Doxorubicin and oxaliplatin also reduced the mitochondrial transmembrane potential ($p < 0.05$). In addition, doxorubicin also caused caspase-3 activation ($p < 0.05$).

The cell cycle distribution in HL-60 cells treated with the complex was assessed by DNA content using flow cytometry after 24 and 48 h of incubation. Table 6 shows the cell cycle distribution obtained. All DNA that was sub-diploid in size (sub-G_0/G_1) was considered fragmented. The treatment with the complex caused a significant increase in the internucleosomal DNA fragmentation in all concentrations and time points analyzed ($p < 0.05$). Doxorubicin also significantly induced internucleosomal DNA fragmentation ($p < 0.05$). Oxaliplatin caused cell cycle arrest at the phase G_2/M that was followed by internucleosomal DNA fragmentation ($p < 0.05$).

The effect of the complex in intracellular ROS levels was investigated in HL-60 cells through flow cytometry using DCFH-DA after 1 and 3 h of incubation. The treatment with the complex for 1 h caused increasing in the ROS levels (Fig. 8). Furthermore, the pretreatment with the antioxidant NAC reduced the complex-induced apoptotic cells (Fig. 9). Since the ROS-mediated cell death can induce activation of the MAPK pathway, we decided to investigate the role of the three main MAPK families, ERK1/2, JNK/SAPK and p38 MAPK, in complex-induced apoptosis in HL-60 cells. Interestingly, the pretreatment with p38 MAPK inhibitor (PD 169316) and MEK inhibitor (U-0126), which inhibits the activation of ERK1/2, but not JNK/SAPK inhibitor (SP 600125), reduced the complex-induced apoptosis (Fig. 10), indicating that the complex causes ROS/ERK/p38-mediated apoptosis in HL-60 cells.

3.4. The complex cis-[PtCl(PIP-OH)(PPh_3)$_2$]PF_6 does not induce DNA intercalation

Since platinum complexes are able to induce DNA intercalation, we evaluated a DNA intercalation assay by examining the ability of the complex to displace ethidium bromide from ctDNA using a cell-free assay. In this assay, if the complex acts as a DNA intercalator, the ethidium bromide fluorescence decrease. However, the complex did not reduce the ethidium bromide fluorescence, indicating that is not a strong DNA intercalator. Doxorubicin, a known DNA intercalator, reduced the fluorescence intensity of ethidium bromide (data not shown).

4. Discussion

In the present work, we synthesized a novel platinum complex containing a piplartine demethylated derivative *cis*-[PtCl(PIP-OH)(PPh_3)$_2$]PF_6 which exhibited an enhanced cytotoxicity in a panel of cancer cells. As mentioned above, metallo-based piplartine complexes had been previously synthesized and evaluated in cancer cells, where the ruthenium-based piplartine complexes displayed more potent cytotoxicity than piplartine [32]. In these ruthenium complexes, piplartine is an uncharged ligand that is coordinated to the ruthenium through the piplartine C=O group. Here, we synthesized a piplartine demethylated derivative PIP-OH to try coordinate the platinum through the hydroxyl group of PIP-OH; however, the ligand PIP-OH coordinated to the platinum through its C=O group. Nevertheless, the platinum-based complex presented more potent cytotoxicity than piplartine and PIP-OH. In both ruthenium and platinum complexes, the ligands piplartine or the piplartine demethylated derivative PIP-OH are dissociated from the metal center, suggesting that in physiology solution, metal complexes can act as a carrier of piplartine [32].

The potent cytotoxic activity of piplartine has been described in different cancer cell lines [9,12,22,23]. Additionally, diverse platinum complexes, including the clinically useful drugs cisplatin, carboplatin and oxaliplatin, have great cytotoxic potential in cancer cell lines [24,31,49,50].

The cytotoxic effect of the platinum-based piplartine complex has been associated with its ability to cause apoptosis in HL-60 cells, as observed by apoptotic cell morphology, increased internucleosomal DNA fragmentation, without cell membrane permeability, loss of the

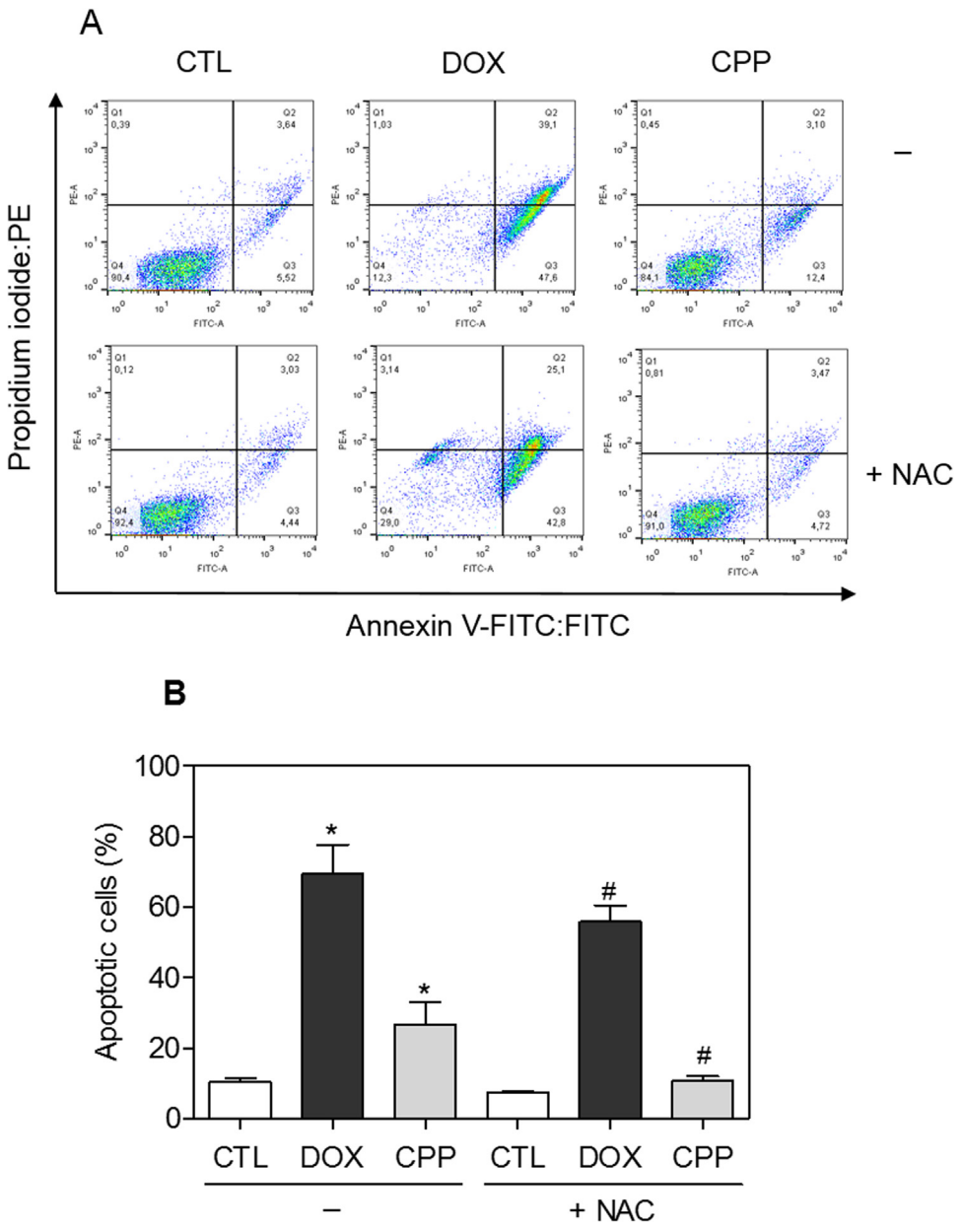

Fig. 9. Effect of the antioxidant *N*-acetyl-*L*-cysteine (NAC) in the apoptosis induced by the complex *cis*-[PtCl(PIP-OH)(PPh_3)$_2$]PF_6 (CPP) in HL-60 cells determined by flow cytometry using annexin V-FITC/PI staining. (**A**) Representative flow cytometric dot plots showing the percentage of cells in viable, early apoptotic, late apoptotic and necrotic stages. (**B**) Quantification of apoptotic HL-60 cells. For protection assay, the cells were pre-treated for 2 h with 5 mM NAC, then incubated with 4 μM CPP for 48 h. The negative control (CTL) was treated with the vehicle (0.1% DMSO) used for diluting the compounds tested. Doxorubicin (DOX, 2 μM) was used as the positive control. Data are presented as the mean ± S.E.M. of three independent experiments performed in duplicate. Ten thousand events were evaluated per experiment and cellular debris was omitted from the analysis. $^{*}P < 0.05$ compared with the negative control by ANOVA followed by Student Newman-Keuls test. # $P < 0.05$ compared with the respective treatment without inhibitor by ANOVA followed by Student Newman-Keuls test.

mitochondrial transmembrane potential, increased phosphatidylserine externalization and caspase-3 activation. Additionally, treatment with the complex also caused a marked increase in the production of ROS, and the pretreatment with the antioxidant NAC, p38 MAPK inhibitor (PD 169316) and MEK inhibitor (U-0126) reduced the complex-induced apoptosis, indicating activation of ROS/ERK/p38-mediated apoptosis pathway.

Piplartine has also been reported to inhibit the proliferation and survival of different leukemia cells. It inhibits the proliferation of B-cell acute lymphoblastic leukemia cell lines, but not for normal B cells, which is achieved by inducing apoptosis via elevation of ROS. The mRNA levels of AURKB, BIRC5, E2F1, and MYB were significantly downregulated, and SOX4 and XBP levels were increased. An increase in the expression of p21 through a p53-independent mechanism was also observed in piplartine treatment [20]. Piplartine also inhibited the viability of bone marrow mononuclear cells from the patients with myeloid leukemias, but not from patients with myelodysplastic syndrome, which induced apoptotic and autophagic cell death via activation of ROS-p38/JNK pathways [22]. Piplartine also reversed doxorubicin resistance in K562/A02 human leukemia cells by PI3K/Akt pathway [21]. Moreover, piplartine also induced apoptosis through activation of ERK signaling in cholangiocarcinoma and colon carcinoma cell lines [51,52].

The platinum-containing drug cisplatin was also previously reported as cytotoxic agent to HL-60 cells, causing nuclear fragmentation, caspase-3 cleavage and phosphatidylserine externalization, which was prevented by NAC and glutathione [53]. Its mode of action has been also associated to its ability to crosslink with the purine bases on the DNA, interfering with DNA repair mechanisms, causing DNA damage, and inducing apoptosis in cancer cells [54]. Here, however, the novel platinum-based piplartine complex produced failed to induce DNA intercalation.

In summary, the complex exhibits more potent cytotoxicity than piplartine in a panel of different cancer cells and triggers ROS/ERK/p38-mediated apoptosis in HL-60 cells. These results imply that although piplartine has undergone structural modifications to form a platinum-based complex and become more potent than piplartine, the mechanism of action appears to be similar to piplartine, since piplartine is also able to cause ROS/ERK/p38-mediated apoptosis in different cancer cells. The formation of this complex represents a new prototype

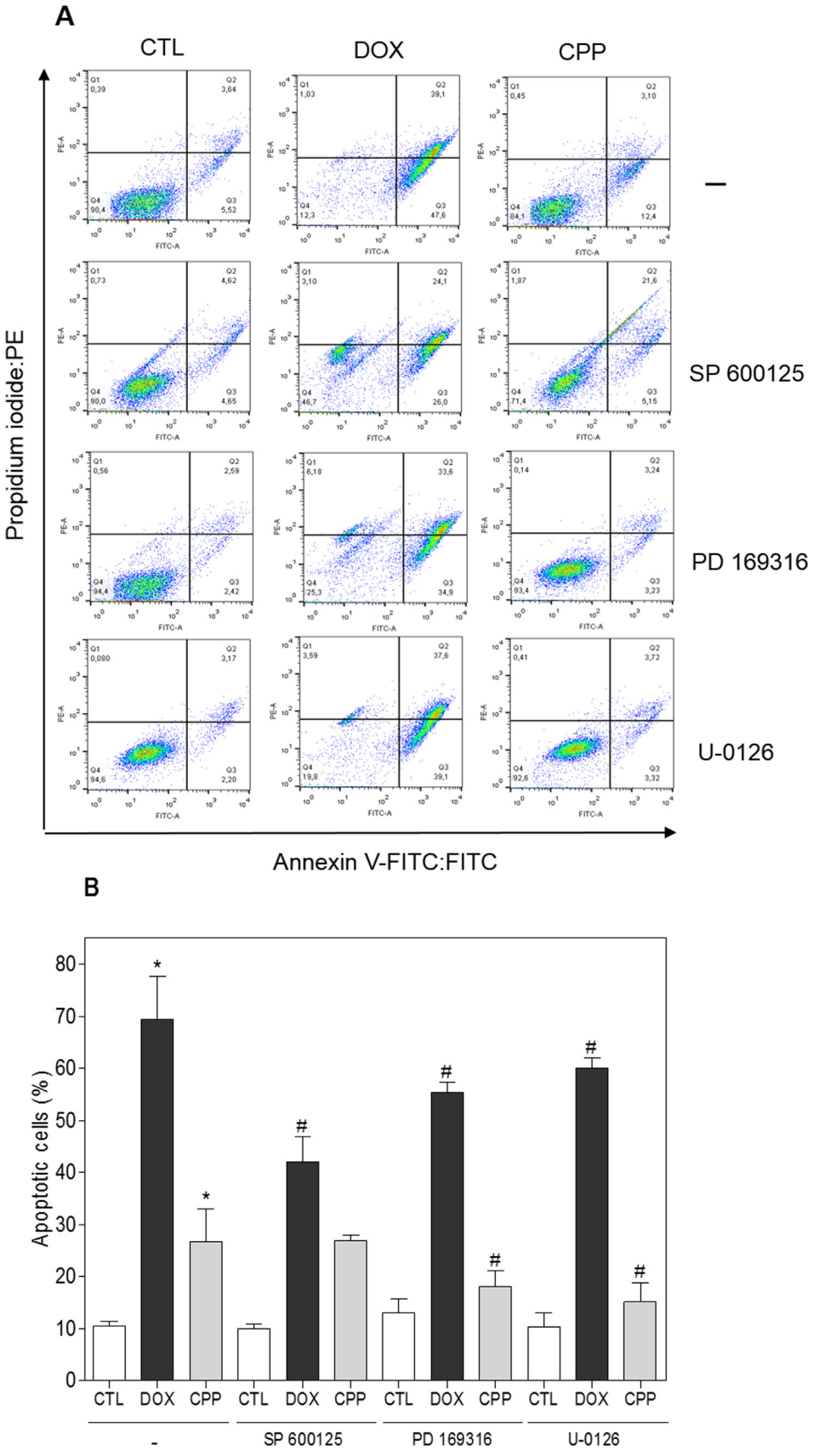

Fig. 10. Effect of the JNK/SAPK inhibitor (SP 600125), p38 MAPK inhibitor (PD 169316) and MEK inhibitor (U-0126) in the apoptosis induced by the complex *cis*-[PtCl(PIP-OH)(PPh_3)$_2$]PF_6 (CPP) in HL-60 cells determined by flow cytometry using Annexin V-FITC/PI staining. (**A**) Representative flow cytometric dot plots showing the percent of cells in the viable, early apoptotic, late apoptotic and necrotic stage. (**B**) Quantification of apoptotic HL-60 cells. For protection assay, the cells were pretreated for 2 h with 5 μM SP 600125, 5 μM PD 169316 or 5 μM U-0126, and then incubated with 4 μM CPP for 48 h. The negative control (CTL) was treated with the vehicle (0.1% DMSO) used for diluting the compound tested. Doxorubicin (DOX, 2 μM) was used as the positive control. Data are presented as the means ± S.E.M. of three independent experiments performed in duplicate. Ten thousand events were evaluated per experiment and cellular debris was omitted from the analysis. * $P < 0.05$ compared with the negative control by ANOVA, followed by the Student-Newman-Keuls test. # $P < 0.05$ compared with the respective treatment without inhibitor by ANOVA, followed by the Student-Newman-Keuls test.

for the development of antitumor drugs.

Acknowledgments

The authors are grateful to the flow cytometry platform of FIOCRUZ-Bahia for collecting the flow cytometric data. This work received financial support and fellowships from Brazilian agencies Conselho Nacional de Desenvolvimento Científico e Tecnológico (CNPq), Fundação de Amparo à Pesquisa de Minas Gerais (FAPEMIG) and Coordenação de Aperfeiçoamento de Pessoal de Nível Superior (CAPES). In special, we also thank CNPq and CAPES for research fellowships (M.I.F.B.; D.R.M.M.; F.T.M.; R.P.M.; A.C.D; M.B.P.S.; D.P.B.).

Appendix A. Supplementary material

Supplementary data associated with this article can be found in the online version at doi:10.1016/j.redox.2018.10.006.

References

[1] L.A. Torre, F. Bray, R.L. Siegel, J. Ferlay, J. Lortet-Tieulent, A. Jemal, Global cancer statistics, 2012, CA Cancer J. Clin. 65 (2015) 87–108.
[2] Cancer Facts & Figures 2017, American Cancer Society, Atlanta, GA, 2017.
[3] D.P. Bezerra, C. Pessoa, M.O. Moraes, E.R. Silveira, M.A. Lima, F.J. Elmiro, L.V. Costa-Lotufo, Antiproliferative effects of two amides, piperine and piplartine, from Piper species, Z. Naturforsch. C 60 (2005) 539–543.
[4] D.P. Bezerra, F.O. Castro, A.P. Alves, C. Pessoa, M.O. Moraes, E.R. Silveira, M.A. Lima, F.J. Elmiro, L.V. Costa-Lotufo, In vivo growth-inhibition of Sarcoma 180 by piplartine and piperine, two alkaloid amides from Piper, Braz. J. Med. Biol. Res. 39 (2006) 801–807.
[5] D.P. Bezerra, G.C. Militão, F.O. Castro, C. Pessoa, M.O. Moraes, E.R. Silveira, M.A. Lima, F.J. Elmiro, L.V. Costa-Lotufo, Piplartine induces inhibition of leukemia cell proliferation triggering both apoptosis and necrosis pathways, Toxicol. Vitr. 21 (2007) 1–8.
[6] D.P. Bezerra, D.J. Moura, R.M. Rosa, M.C. Vasconcellos, A.C. Silva, M.O. Moraes, E.R. Silveira, M.A. Lima, J.A. Henriques, L.V. Costa-Lotufo, J. Saffi, Evaluation of the genotoxicity of piplartine, an alkamide of *Piper tuberculatum*, in yeast and mammalian V79 cells, Mut. Res. 652 (2008) 164–174.
[7] D.P. Bezerra, F.O. Castro, A.P. Alves, C. Pessoa, M.O. Moraes, E.R. Silveira, M.A. Lima, F.J. Elmiro, N.M. Alencar, R.O. Mesquita, M.W. Lima, L.V. Costa-Lotufo, In vitro and in vivo antitumor effect of 5-FU combined with piplartine and piperine, J. Appl. Toxicol. 28 (2008) 156–163.
[8] D.P. Bezerra, M.C. Vasconcellos, M.S. Machado, I.V. Villela, R.M. Rosa, D.J. Moura, C. Pessoa, M.O. Moraes, E.R. Silveira, M.A. Lima, N.C. Aquino, J.A. Henriques, J. Saffi, L.V. Costa-Lotufo, Piplartine induces genotoxicity in eukaryotic but not in prokaryotic model systems, Mut. Res. 677 (2009) 8–13.
[9] K.V. Golovine, P.B. Makhov, E. Teper, A. Kutikov, D. Canter, R.G. Uzzo, V.M. Kolenko, Piperlongumine induces rapid depletion of the androgen receptor in human prostate cancer cells, Prostate 73 (2013) 23–30.
[10] D.P. Bezerra, C. Pessoa, M.O. Moraes, L.V. Costa-Lotufo, D.R. Gouvea, V.A.P. Jabor, N.P. Lopes, K.B. Borges, M.A.S. Lima, E.R. Silveira, Sensitive method for determination of piplartine, an alkaloid amide from piper species, in rat plasma samples by liquid chromatography-tandem mass spectrometry, Quim. Nova 35 (2011) 460–465.
[11] D.J. Adams, M. Dai, G. Pellegrino, B.K. Wagner, A.M. Stern, A.F. Shamji, S.L. Schreiber, Synthesis, cellular evaluation, and mechanism of action of piperlongumine analogs, Proc. Natl. Acad. Sci. USA 109 (2012) 15115–15120.
[12] D.P. Bezerra, C. Pessoa, M.O. de Moraes, N. Saker-Neto, E.R. Silveira, L.V. Costa-Lotufo, Overview of the therapeutic potential of piplartine (piperlongumine), Eur. J. Pharm. Sci. 48 (2013) 453–463.
[13] D.P. Bezerra, P.M. Ferreira, C.M. Machado, N.C. de Aquino, E.R. Silveira, R. Chammas, C. Pessoa, Antitumour efficacy of *Piper tuberculatum* and piplartine based on the hollow fiber assay, Planta Med. 81 (2015) 15–19.
[14] F.L. Moreira, M.D. Habenschus, T. Barth, L.M. Marques, A.C. Pilon, V.S. Bolzani, R. Vessecchi, N.P. Lopes, A.R. Oliveira, Metabolic profile and safety of piperlongumine, Sci. Rep. 6 (2016) 33646.
[15] A.M. Fregnan, G.A. Brancaglion, A.F.C. Galvão, C.O.S. Costa, D.R.M. Moreira, M.B.P. Soares, D.P. Bezerra, N.C. Silva, S.M.S. Morais, J.C. Oliver, A.L.T. Dias, L.F.L. Coelho, D.T. Carvalho, D.F. Dias, T.B. Souza, Synthesis of piplartine analogs and preliminary findings on structure–antimicrobial activity relationship, Med. Chem. Res. 26 (2017) 603–614.
[16] J. Mohammad, H. Dhillon, S. Chikara, S. Mamidi, A. Sreedasyam, K. Chittem, M. Orr, J.C. Wilkinson, K.M. Reindl, Piperlongumine potentiates the effects of gemcitabine in in vitro and in vivo human pancreatic cancer models, Oncotarget 9 (2017) 10457–10469.
[17] F. Dai, C.H. Yuan, Y. Ji, Y.T. Du, X.Z. Bao, L.X. Wu, X.L. Jin, B. Zhou, Keto-enol-based modification on piperlongumine to generate a potent Cu(II) ionophore that triggers redox imbalance and death of HepG2 cells, Free Radic. Biol. Med. 120 (2018) 124–132.
[18] Y. Zou, D. Zhao, C. Yan, Y. Ji, J. Liu, J. Xu, Y. Lai, J. Tian, Y. Zhang, Z. Huang, Novel Ligustrazine-based analogs of piperlongumine potently suppress proliferation and metastasis of colorectal cancer cells in vitro and in vivo, J. Med. Chem. 61 (2018) 1821–1832.
[19] W. Hang, Z.X. Yin, G. Liu, Q. Zeng, X.F. Shen, Q.H. Sun, D.D. Li, Y.P. Jian, Y.H. Zhang, Y.S. Wang, C.S. Quan, R.X. Zhao, Y.L. Li, Z.X. Xu, Piperlongumine and p53-reactivator APR-246 selectively induce cell death in HNSCC by targeting GSTP1, in press, Oncogene (2018), https://doi.org/10.1038/s41388-017-0110-2.
[20] S.S. Han, S. Han, N.L. Kamberos, Piperlongumine inhibits the proliferation and survival of B-cell acute lymphoblastic leukemia cell lines irrespective of glucocorticoid resistance, Biochem. Biophys. Res. Commun. 452 (2014) 669–675.
[21] Q. Kang, S. Yan, Piperlongumine reverses doxorubicin resistance through the PI3K/Akt signaling pathway in K562/A02 human leukemia cells, Exp. Ther. Med. 9 (2015) 1345–1350.
[22] X.X. Xiong, J.M. Liu, X.Y. Qiu, F. Pan, S.B. Yu, X.Q. Chen, Piperlongumine induces apoptotic and autophagic death of the primary myeloid leukemia cells from patients via activation of ROS-p38/JNK pathways, Acta Pharmacol. Sin. 36 (2015) 362–374.
[23] Y. Liao, X. Niu, B. Chen, H. Edwards, L. Xu, C. Xie, H. Lin, L. Polin, J.W. Taub, Y. Ge, Z. Qin, Synthesis and antileukemic activities of piperlongumine and HDAC inhibitor hybrids against acute myeloid leukemia cells, J. Med. Chem. 59 (2016) 7974–7990.
[24] Z. Xu, W. Hu, Z. Wang, S. Gou, Platinum(IV) prodrugs multiply targeting genomic DNA, histone deacetylases and PARP-1, Eur. J. Med. Chem. 141 (2017) 211–220.
[25] V.R. Silva, R.S. Corrêa, L.S. Santos, M.B.P. Soares, A.A. Batista, D.P. Bezerra, A ruthenium-based 5-fluorouracil complex with enhanced cytotoxicity and apoptosis induction action in HCT116 cells, Sci. Rep. 8 (2018) 288.
[26] N.C. Carvalho, S.P. Neves, R.B. Dias, L.F. Valverde, C.B.S. Sales, C.A.G. Rocha, M.B.P. Soares, E.R. Dos Santos, R.M.M. Oliveira, R.M. Carlos, P.C.L. Nogueira, D.P. Bezerra, A novel ruthenium complex with xanthoxylin induces S-phase arrest and causes ERK1/2-mediated apoptosis in HepG2 cells through a p53-independent pathway, Cell Death Dis. 9 (2018) 79.
[27] R.S. Correa, V. Freire, M.I.F. Barbosa, D.P. Bezerra, L.M. Bomfim, D.R.M. Moreira, M.B.P. Soares, J. Ellena, A.A. Batista, Ru(II)-thyminate complexes: new metallodrug candidates against tumor cells, New J. Chem. 42 (2018) 6794–6802.
[28] M.S. Oliveira, A.A.D. Santana, R.S. Correa, M.B.P. Soares, A.A. Batista, D.P. Bezerra, Ru(II)-thymine complex causes cell growth inhibition and induction of caspase-mediated apoptosis in human promyelocytic leukemia HL-60 cells, Int. J. Mol. Sci. 19 (2018) E1609.
[29] W. Zhou, M. Almeqdadi, M.E. Xifaras, I.A. Riddell, Ö.H. Yilmaz, S.J. Lippard, The effect of geometric isomerism on the anticancer activity of the monofunctional platinum complex trans-[$Pt(NH_3)_2$(phenanthridine)Cl]NO_3, Chem. Commun. 54 (2018) 2788–2791.
[30] W. Hua, J. Zhao, W. Hu, S. Gou, Combination of 7-hydroxycoumarin in a platinum (IV) complex derived from cisplatin enhanced cytotoxicity with multiple mechanisms of action, J. Inorg. Biochem. 186 (2018) 17–23.
[31] M. Zaki, F. Arjmand, S. Tabassum, Current and future potential of metallo drugs: revisiting DNA-binding of metal containing molecules and their diverse mechanism of action, Inorg. Chim. Acta 444 (2016) 1–22.
[32] C.O.D. Costa, J.H. Araujo-Neto, I.R.S. Baliza, R.B. Dias, L.F. Valverde, M.T.A. Vidal, C.B.S. Sales, C.A.G. Rocha, D.R.M. Moreira, M.B.P. Soares, A.A. Batista, D.P. Bezerra, Novel piplartine-containing ruthenium complexes: synthesis, cell growth inhibition, apoptosis induction and ROS production on HCT116 cells, Oncotarget 8 (2017) 104367–104392.
[33] APEX2, Bruker AXS Inc., Madison, Wisconsin, USA, 2009.
[34] L. Krause, R. Herbst-Irmer, G.M. Sheldrick, D. Stalke, Comparison of silver and molybdenum microfocus X-ray sources for single-crystal structure determination, J. Appl. Crystallogr 48 (2015) 3–10.
[35] G.M. Sheldrick, Crystal structure refinement with SHELXL, Acta Cryst. 71 (2015) 3–8.
[36] L.J. Farrugia, WinGX suite for small-molecule single-crystal crystallography, J. Appl. Crystallogr. 32 (1999) 837.
[37] L.J. Farrugia, ORTEP-3 for windows – a version of ORTEP-III with a graphical user interface (GUI), J. Appl. Crystallogr. 30 (1997) 565.
[38] S.A. Ahmed, R.M. Gogal, J.E. Walsh, A new rapid and simple non-radioactive assay to monitor and determine the proliferation of lymphocytes an alternative to [^{3}H] thymidine incorporation assay, J. Immunol. Methods 170 (1994) 211–224.
[39] L.S. Santos, V.R. Silva, L.R.A. Menezes, M.B.P. Soares, E.V. Costa, D.P. Bezerra, Xylopine induces oxidative stress and causes G_2/M Phase arrest, triggering caspase-mediated apoptosis by p53-independent pathway in HCT116 cells, Oxid. Med. Cell. Longev. 2017 (2017) 7126872.
[40] R.B. Dias, T.B.S. de Araújo, R.D. de Freitas, A.C.B.D.C. Rodrigues, L.P. Sousa, C.B.S. Sales, L.F. Valverde, M.B.P. Soares, M.G. Dos Reis, R.D. Coletta, E.A.G. Ramos, C.A. Camara, Silva TMS, J.M.B. Filho, D.P. Bezerra, C.A.G. Rocha, β-Lapachone and its iodine derivatives cause cell cycle arrest at G_2/M phase and reactive oxygen species-mediated apoptosis in human oral squamous cell carcinoma cells, Free Radic. Biol. Med. 126 (2018) 87–100.
[41] F.X. Sureda, E. Escubedo, C. Gabriel, J. Comas, J. Camarasa, A. Camins, Mitochondrial membrane potential measurement in rat cerebellar neurons by flow cytometry, Cytometry 28 (1997) 74–80.
[42] I. Nicoletti, G. Migliorati, M.C. Pagliacci, F. Grignani, C. Riccardi, A rapid and simple method for measuring thymocyte apoptosis by propidium iodide staining and flow cytometry, J. Immunol. Methods 139 (1991) 271–279.
[43] C.P. LeBel, H. Ischiropoulos, S.C. Bondy, Evaluation of the probe 2′,7′-dichlorofluorescin as an indicator of reactive oxygen species formation and oxidative stress, Chem. Res. Toxicol. 5 (1992) 227–231.
[44] L.S. Glass, A. Bapat, M.R. Kelley, M.M. Georgiadis, E.C. Long, Semi-automated high-throughput fluorescent intercalator displacement-based discovery of cytotoxic DNA binding agents from a large compound library, Bioorg. Med. Chem. Lett. 20 (2010)

1685–1688.
[45] W.J. Geary, The use of conductivity measurements in organic solvents for the characterisation of coordination compounds, Coord. Chem. Rev. 7 (1971) 81–122.
[46] K. Nakamoto, Infrared and Raman Spectra of Inorganic and Coordination Compounds, 5th edition, Wiley-Interscience, New York, NY, 2008.
[47] J.S. Oliveira, D.P. Bezerra, C.D.T. Freitas, J.D.B. Marinho-Filho, M.O. Moraes, C. Pessoa, L.V. Costa-Lotufo, M.V. Ramos, In vitro cytotoxicity against different human cancer cell lines of laticifers proteins of *Calotropis procera* (Ait.) R.Br, Toxicol. Vitr. 21 (2007) 1563–1573.
[48] A.K. Calgarotto, V. Maso, G.C.F. Junior, A.E. Nowill, P.L. Filho, J. Vassallo, S.T.O. Saad, Antitumor activities of quercetin and green tea in xenografts of human leukemia HL60 cells, Sci. Rep. 8 (2018) 3459.
[49] N. Muhammad, N. Sadia, C. Zhu, C. Luo, Z. Guo, X. Wang, Biotin-tagged platinum (iv) complexes as targeted cytostatic agents against breast cancer cells, Chem. Commun. 53 (2017) 9971–9974.
[50] E. Bauer, X. Domingo, C. Balcells, I.H. Polat, M. Crespo, J. Quirante, J. Badía, L. Baldomà, M. Font-Bardia, M. Cascante, Synthesis, characterization and biological activity of new cyclometallated platinum(iv) iodido complexes, Dalton Trans. 46 (2017) 14973–14987.
[51] H. Randhawa, K. Kibble, H. Zeng, M.P. Moyer, K.M. Reindl, Activation of ERK signaling and induction of colon cancer cell death by piperlongumine, Toxicol. Vitr. 27 (2013) 1626–1633.
[52] S. Thongsom, W. Suginta, K.J. Lee, H. Choe, C. Talabnin, Piperlongumine induces G2/M phase arrest and apoptosis in cholangiocarcinoma cells through the ROS-JNK-ERK signaling pathway, Apoptosis 22 (2017) 1473–1484.
[53] M. Previati, I. Lanzoni, E. Corbacella, S. Magosso, V. Guaran, A. Martini, S. Capitani, Cisplatin-induced apoptosis in human promyelocytic leukemia cells, Int. J. Mol. Med. 18 (2006) 511–516.
[54] S. Dasari, P.B. Tchounwou, Cisplatin in cancer therapy: molecular mechanisms of action, Eur. J. Pharmacol. 740 (2014) 364–378.